Nanotechnology **22** (2011) 235704 (9pp) doi:10.1088/0957-4484/22/23/235704

Electro-optic investigation of the surface trapping efficiency in *n*-alkanethiol SAM passivated GaAs(001)

Gregory M Marshall[1,2], **Gregory P Lopinski**[3], **Farid Bensebaa**[2] and **Jan J Dubowski**[1,4]

[1] Department of Electrical and Computer Engineering, Université de Sherbrooke, Sherbrooke, QC, J1K 2R1, Canada
[2] Institute for Chemical Process and Environmental Technology, National Research Council of Canada, Ottawa, ON, K1A 0R6, Canada
[3] Steacie Institute for Molecular Sciences, National Research Council of Canada, Ottawa, ON, K1A 0R6, Canada

E-mail: jan.j.dubowski@usherbrooke.ca

Received 14 February 2011, in final form 19 March 2011
Published 14 April 2011
Online at stacks.iop.org/Nano/22/235704

Abstract
The electro-optic characteristics of the semi-insulating and n^+-type GaAs(001) surfaces passivated with *n*-alkanethiol self-assembled monolayers were investigated using Kelvin probe surface photovoltage (SPV) and photoluminescence (PL) techniques. Referencing the equilibrium surface barrier height established in an earlier report, SPV measurements demonstrated a significant (>100 mV) increase in the non-equilibrium band-bending potential observed under low-level photo-injection. Modeling of the SPV accounts for these observations in terms of a large ($>10^4$) decrease in the hole/electron ratio of surface carrier capture cross-sections, which is suggested to result from the electrostatic potential of the interfacial dipole layer formed upon thiol chemisorption. The cross-section effects are verified in the high-injection regime based on carrier transport modeling of the PL enhancement manifested as a reduction of the surface recombination velocity.

1. Introduction

Semiconductor surfaces coupled to molecular structures derived from organic chemistry are currently being developed for a variety of molecular electronic and sensor applications in the electronic and optical domains. For example, self-assembled monolayers (SAMs) form the basis of molecular junctions suitable for the investigation of electronic transport properties [1–4], or can support various recognition elements in biosensor applications [5–8]. Of particular interest are SAMs comprised of *n*-alkanethiols [$HS(CH_2)_nR$], which are known for their ability to interface with the GaAs(001) surface through S–GaAs covalent bond formation [9–14]. The passivating effects of this surface treatment have been reported in terms of photoluminescence (PL) enhancements [15–18], relative surface Fermi level (FL) changes [19, 20], and chemical stabilization with respect to the regrowth of surface oxides [21, 22]. Quantitative understanding has been limited to estimates of the decrease in surface recombination velocity (SRV), which is a fundamental parameter of the surface derived from Shockley–Read–Hall recombination theory. In the comprehensive study by Lunt *et al* [18], SRV reduction was determined to be a significant factor contributing to PL enhancement in sulfide-treated GaAs, including the organic thiols. This conclusion was based on time-resolved PL under high-injection conditions, where an increase in carrier lifetime implied a decrease in the trap density or carrier capture cross-section of the relevant surface states. However, distinction between the effects of a decrease in these two factors cannot readily be made without prior knowledge of the equilibrium band-bending, a characteristic of defect passivation only. See figure 1 for a schematic representation of the n-type GaAs surface band structure shown in depletion.

[4] Author to whom any correspondence should be addressed.

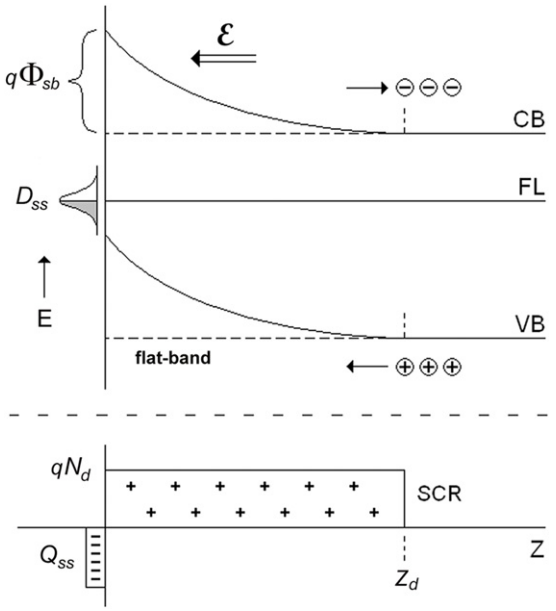

Figure 1. Surface band structure of n-type GaAs. Symbols: space charge density (qN_d), space charge region (SCR), depletion depth (z_d), surface trapped charge (−), ionized donors (+), surface acceptor state density (Q_{ss}), Fermi level energy (FL), conduction/valence band-edges (CB/VB), surface potential barrier height ($q\Phi_{sb}$), built-in electric field ($\mathcal{E}$) and energy density of surface states (D_{ss}). Photo-generated excess minority carriers (⊕) are driven into the SCR by drift and diffusion processes contributing to the non-radiative SRV.

In previous work, we used x-ray photoelectron spectroscopy (XPS) to establish the precise surface FL energy and, therefore, the equilibrium band-bending before and after the formation of hexadecanethiol [$HS(CH_2)_{15}CH_3$] SAMs (n_{15}-SAMs) [23]. Passivation of the electronically active defect levels was small, i.e., unpinning of the surface FL was limited to less than 50 meV, meaning that only small changes to the surface trapped charge density were realized. This lends further support to the SRV model of PL enhancement by rejecting a dead-layer model explanation [24], which calls for a more substantial relocation of the surface FL and corresponding reduction of the depletion depth. More importantly, it suggests that the capture cross-sections play a significant role in the change of the non-radiative recombination rate at the thiolated surface. Quantitatively, it was determined that for undoped semi-insulating (SI) GaAs, the surface FL was located at 0.21–0.26 eV above the valence band-edge, indicating the presence of a high density of surface acceptors and a surface barrier height ($q\Phi_{sb}$) of 0.51–0.56 eV, which is consistent with both the Ga-rich surface stoichiometry observed after etching [10], and ionization of the EL2 deep level donor (As_{Ga} antisite defect) in its typical bulk concentration ($\sim 10^{16}$ cm^{-3}) [25, 26]. Similarly, the surface barrier height in heavily Si-doped (n^+-type) GaAs was determined to be 0.76–0.78 eV, based on a surface FL located at 0.69–0.71 eV and ionization in the space charge region (SCR) according to the nominal doping concentration ($\sim 10^{18}$ cm^{-3}). Furthermore, it was noted these surface characteristics conform to those prescribed by the advanced unified defect model (AUDM) [27].

In this paper, we extend our investigation of this material system into the non-equilibrium domain by employing surface photovoltage (SPV) techniques, PL measurements and numerical analyses in order to distinguish the effects of the carrier capture cross-sections from those of the surface trap density. By referencing the initial band-bending previously determined by XPS, SPV modeling is used in order to highlight large scale changes to the hole/electron ratio of surface capture cross-sections, which specifies the degree of surface charge modification under photo-excitation. Observations of the residual band-bending under low-injection conditions are understood in this context, and are discussed in terms of the effect the interfacial dipole layer formed by thiol–GaAs chemisorption has on minority carrier dynamics. The cross-section effects are then verified in the high-injection regime based on carrier transport modeling of the PL enhancement following thiol passivation, which is manifested as a reduction of the SRV.

2. Experimental details

2.1. Sample preparation

Details on the preparation of *n*-alkanethiol SAMs have been reported elsewhere [28]. SI-GaAs(001) epi-ready wafer was used for this study in addition to heavily doped n^+-GaAs (Si-doped at 1×10^{18} cm^{-3}) for comparative analysis. Reference samples were prepared following 28% NH_4OH/H_2O etching by immersion in degassed ethanol solvent without alkanethiol. Samples were prepared under N_2 purged glovebox conditions and were stored under N_2 until tested (SPV < 2 h, PL < 6 h), thus representing the initial condition of the passivated surface immediately following SAM preparation without significant oxide ageing [28].

2.2. SPV

The Kelvin probe instrument (KP Technology Ltd) records the contact potential difference (CPD) with respect to a non-contact vibrating Au reference probe. Single point measurements were made using a 2 mm probe diameter and front/back surface grounding contacts. Electronic drift caused by stray capacitance was minimized by the use of a Faraday cage enveloping the Kelvin probe unit. SPV measurements were obtained by monitoring the change in CPD upon glancing illumination from a cold white light source (fiber-optic illuminator). The SPV is defined as the variation of CPD in dark versus light exposed conditions (SPV $= \Delta CPD_{d-l}$). Light modulation periods were manually determined in order to demonstrate reproducible cycling of the CPD. A thermopile detector was used to estimate the total optical power emitted from the fiber-optic (175 mW), projecting a transmitted irradiance of about 10^{17} photons cm^{-2} s^{-1} through the GaAs surface, accounting for beam geometric factors and surface reflection.

2.3. PL

A stepping stage PL mapper (Philips Electronics Ltd PLM-150) was used at an excitation wavelength of 532 nm

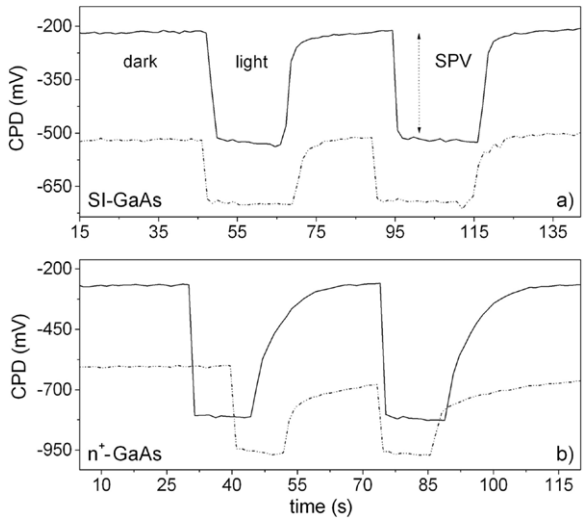

Figure 2. Top: Kelvin probe SPV measurements on SI-GaAs; etched only GaAs (solid), GaAs prepared with n_{15}-SAM (dash-dot). Light conditions refer to white light illumination with a fiber-optic coupled quartz halogen lamp at an irradiance of 10^{17} photons cm^{-2} s^{-1}. The SPV is quantified as the change in CPD. Bottom: similar measurements on n$^+$-GaAs.

and incident power of 32 mW in an estimated 10 μm Gaussian mode field diameter (2×10^{23} photons cm^{-2} s^{-1}). Measurements were stepped in 100–200 μm increments with dwell times on the order of 100 ms. The peak PL intensity was recorded at the emission maximum near 870 nm. A data filter was later used to extract the sampling average and standard deviation from the center 2–4 mm diameter on each wafer so as to exclude sample edge effects. In addition, neutral density filters were used to vary the excitation power in order to derive the PL efficiency from SI-GaAs.

3. SPV observations and analysis

3.1. SPV results

In a depleted n-type surface, the potential drop across the SCR is negative, and since the SPV represents a reduction in the surface barrier, the SPV is positive valued. This manifests as a reduction of the work function and an increased CPD with respect to the Au probe referenced at 0 mV. Results for SI and n$^+$ material are shown in figures 2(a) and (b) respectively. In each case, the dark condition work function is approximately 310–330 mV lower for the samples prepared with n_{15}-SAMs. This is due to the addition of a dipole layer potential formed by the SAM having a net dipole moment directed outward [29]. Evidence of the repopulation of surface states in the transient return to the equilibrium surface potential can also be seen. More importantly, note that the SPV values are reduced for surfaces prepared with n_{15}-SAMs when compared to their respective reference surfaces. The SPV reduction on SI-GaAs measures 134 mV in figure 2(a) and is 187 mV for n$^+$-GaAs in figure 2(b). In repeated experiments, SPV reductions for n_{15}-SAMs averaged 148 mV and 185 mV for SI and n$^+$-type surfaces respectively, with a standard error of about $\pm$30 mV.

The SPV is governed, in part, by the screening effect photo-generated excess carriers have on the surface trapped charge, which results in a reduction of the surface barrier. In principle, under sufficiently strong photo-injection, the SCR is completely suppressed, leading to SPV saturation and the flat-band condition. However, SPV saturation cannot always be observed in GaAs because of the possible additive contribution of the Dember potential, the interference from which depends on the ratio of hole and electron capture coefficients at the surface, and which is a strong function of irradiance in the high-injection regime [30]. Therefore, we assign the SPV saturation potentials according to the equilibrium surface barrier potentials (Φ_{sb}) derived from our XPS results, since they are directly equivalent but opposite in sign. In this case, we note that Φ_{sb} is at least 200 mV greater than the measured SPV magnitudes and conclude, therefore, that these SPV results do not reflect photo-saturation conditions in the SCR (i.e., flat bands). Consequently, the reduction of SPV indicated for the passivated surfaces, which is at least 100 mV, is interpreted as a relative increase in the residual non-equilibrium band-bending potential under equivalent irradiance conditions.

3.2. SPV model

The screening effect of excess carriers on the SCR is modeled according to Garrett and Brattain [31], and Johnson [32]. In the depletion approximation, the surface space charge density (Q_{sc}) is defined within the depletion depth z_d and may be written

$$Q_{sc} = \sqrt{2kT\ \varepsilon_s n_i}\, F \tag{1}$$

where F is a dimensionless function, which for n-type material can be written as

$$F = [\Psi(e^{-\Omega} + \Omega - 1) + \Psi^{-1}(e^{\Omega} - \Omega - 1) + \Psi^{-1}(e^{\Omega} + e^{-\Omega} - 2)\delta_n]^{\frac{1}{2}} \tag{2}$$

with doping factor $\Psi = \sqrt{p_o/n_o}$ specified by the equilibrium free carrier concentrations. The dimensionless value $\Omega = q\,\Phi/kT$ represents the steady-state, non-equilibrium band-bending under photo-excitation when the fractional excess electron density is $\delta_n = \Delta n/n_o$.

In addition to the screening effect, the SPV is governed by the population of surface states, more specifically, the so-called fast trap states [32], which have surface trap density (N_t) and occupation statistics corresponding to Shockley–Read–Hall surface recombination. These states are ionized based on their energy level (E_t) within the band-gap and the relative position of the surface FL as it varies according to the degree of photo-induced band-flattening. The surface electron and hole capture coefficients, determined by their respective capture cross-sections and thermal velocities ($C_{n,p} = \sigma_{n,p}\ \nu_{th\ n,p}$), also factor into the Shockley–Read–Hall process and contribute to the overall surface state occupation. For example, expressed as a ratio of hole/electron capture coefficients, a decrease in the carrier capture ratio ($\chi^2 = C_p/C_n$) for the depleted surface will result in a smaller SPV at a given excess carrier density because of the persistence of negative surface charge. The

factor χ can vary over several orders of magnitude for surface states, depending on the charge and local potential [24, 33].

The analytical treatment used in our surface state modeling is based on Johnson [32], and Kronik and Shapira [33], and follows the numerical approach used by Aphek *et al* [30]. For an acceptor state, the electron occupancy factor (f_e) is defined in terms of the following:

$$f_e = \left[1 + e^{-(\Phi - \ln\Psi + \nu)}\left(\frac{1 + \Gamma(1+\delta_n)(1+\Psi^{-2}\delta_n)}{(1+\Gamma)(1+\delta_n)}\right)\right]^{-1} \quad (3a)$$

$$\Gamma = \frac{\chi e^{2\nu} e^{-(\Phi - \ln\Psi + \nu)}}{1+\delta_n} \quad (3b)$$

$$\nu = (E_g/2 - E_t)kT^{-1} \quad (3c)$$

where E_g is the band-gap energy. The surface state charge density can then be written as

$$Q_{ss} = -qN_t f_e. \quad (4)$$

Using (1)–(4) and applying the charge neutrality condition,

$$Q_{ss} + Q_{sc} = 0 \quad (5)$$

one may obtain SPV $= (\Omega - \Omega_{sb})kT/q$ by solving (5) for Ω, subject to χ. In the above approach, a single discrete state defect is assumed. Although a continuous distribution of surface state energies may be considered, this simplifying assumption is justified based on our previously reported observations of surface FL pinning [23], which are consistent with the discrete defects prescribed by the AUDM.

3.3. Model parameters

We take E_t from the equilibrium surface FL position of the etched but untreated SI-GaAs surface located at 0.21 eV above the valence band-edge and assign it to an acceptor state. Defined as such, E_t is assumed to be the dominant surface defect level for both material types in accordance with a Ga-rich stoichiometry. Neutral donor states that raise the surface FL near mid-gap in n^+-GaAs are considered much lower in density and are ignored in the charge balance of (5).

In order to fulfil the parameter requirement N_t for acceptor states in (4), the surface charge density in the discrete state FL pinning condition at thermal equilibrium (Q^o_{ss}) is required. Consider the value of Q^o_{ss} as the energy density of surface states D_{ss} (eV^{-1} cm^{-2}) approaches the upper limit,

$$\lim_{D_{ss}\to\infty} q D_{ss}\, dE = Q^o_{ss} \quad (6)$$

where dE is the energy bandwidth differential associated with the discrete state. In thermal equilibrium ($\delta_n = 0$), (1) may be written as

$$Q^o_{sc} = \sqrt{2\varepsilon N_{sc} q \Phi_{sb}}. \quad (7)$$

Using charge neutrality, (6) and (7) are equated and the limit is evaluated. See figure 3 for a graphical representation of solutions for the space charge densities (N_{sc}) and equilibrium surface barriers ($q\,\Phi_{sb}$) corresponding to SI and n^+-type GaAs. The surface trap densities were established by dividing the respective values of Q^o_{ss} by their occupation factors (f_e^{SI}, f_e^{n+}) at equilibrium yielding values of $N_t = 2.1 \times 10^{12}$ cm^{-2} for SI-GaAs and $N_t = 3.3 \times 10^{12}$ cm^{-2} for n^+-type GaAs. These results are satisfactory by virtue of their equivalence, which may be expected for discrete stoichiometric defects.

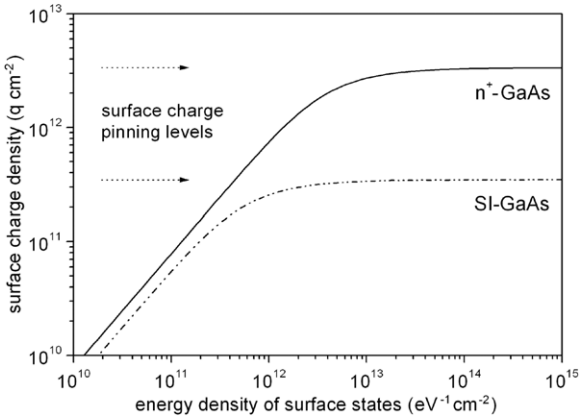

Figure 3. Surface FL pinning places an upper boundary on the surface charge density as the energy density of surface states approaches the discrete limit. Pinning is defined such that further increases in the density of surface states does not change the band-bending.

Table 1. SI-GaAs physical constants used in calculations.

Hole diffusion constant	D_p	10	$cm^2\ s^{-1}$
Hole diffusion length[a]	L_p	1.3×10^{-4}	cm
Absorption coefficient	α_{ex}	7.6×10^4	cm^{-1}
Fresnel reflectance[b]	R	0.29	—
Radiative rate constant	β	2×10^{-10}	$cm^3\ s^{-1}$

[a] Adapted from [35] and [36].
[b] Polarization averaged, estimated at 75° incidence and 532 nm.

3.4. Transformation of scale to photon irradiance

In order to relate the SPV model to the experimental conditions, mapping of the incident photon irradiance (I_{rad}) to the excess carrier density ($\Delta n = \Delta p$) is required. Use is made of the Moss equation, as detailed in the review by Schroder [34], and as similarly employed by Aphek [30]. The Moss equation is a function of the fractional excess electron density (δ_n) and the effective SRV (S_{eff}) at the SCR edge,

$$I_{rad} = \left(\frac{\delta_n n_o}{1-R}\right)\left(S_{eff} + \frac{D_p}{L_p}\right)\left(1 + \frac{1}{\alpha L_p}\right). \quad (8)$$

Typical GaAs values for the remaining parameters are defined in table 1. The variable S_{eff} represents the diffusion flux with which minority carriers move into the SCR, where they are swept to the surface by the built-in field. Since the diffusion current is coupled to the drift current associated with the surface potential, S_{eff} is dependent on the non-equilibrium band-bending. For SI-GaAs, a value of $S^{SI}_{eff} = 1.5 \times 10^5$ cm s^{-1} is assigned, and for n^+-GaAs a value of $S^{n+}_{eff} = 2 \times 10^6$ cm s^{-1} is used. These values follow the

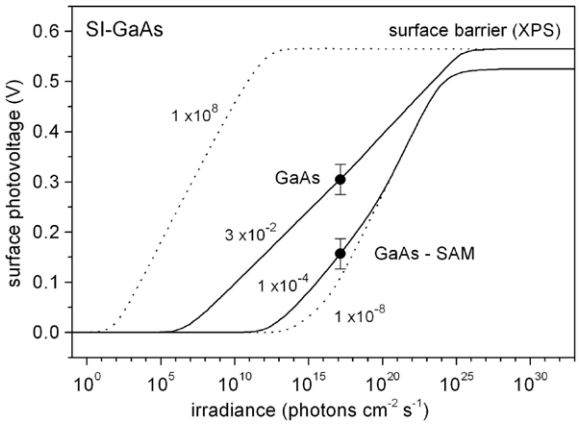

Figure 4. SPV data (circles) and model results for SI-GaAs before and after passivation with n_{15}-SAM. Numerical values indicate the parameter χ used in the SPV calculations (solid). Limiting envelopes of the SPV function at $\chi = 10^{\pm 8}$ (dotted). Exclusive of the Dember potential, the SPV saturates under high level photo-injection with a magnitude equal to the equilibrium surface barrier determined independently by XPS.

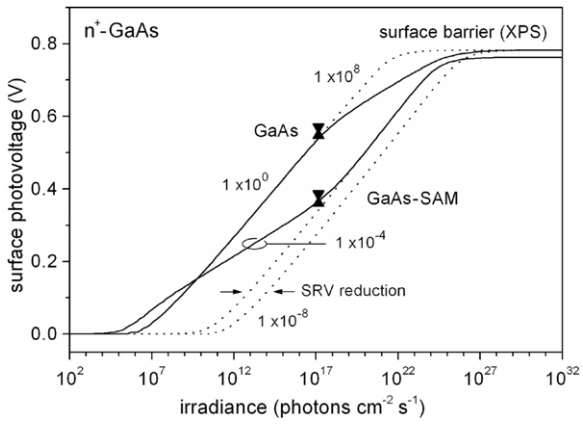

Figure 5. SPV data and model results for n^{+}-GaAs before and after passivation with n_{15}-SAM. Details as per figure 4. Up/down triangles represent individual test results. The indicated curve shifting left reflects the increase in excess carrier density due to a reduction of the SRV for the passivated surface.

low-injection trends in Aspnes [35] and Mettler [36], which correspond to the variation of SRV with doping concentration, or equivalently, the SCR density. A limiting value of δ_n is defined where $S_{\text{eff}} \ll D_p/L_p$, i.e., further reductions of S_{eff} will not produce larger values of δ_n at a given I_{rad}.

3.5. Variation of the carrier capture cross-sections

With the above analytical treatment, the SPV is now calculated as a function of I_{rad} and compared to the experimental SPV data under the constraint that the saturation SPV is equated with the surface barrier height as previously determined by XPS. Figure 4 shows the modeling results for SI-GaAs in which the SPV is plotted across a range of χ values. The dotted lines represent the SPV envelope functions [30]. For example, at $\chi = 10^{8}$, hole capture dominates the modification of surface charge at minimum injection levels and leads to saturation of the SPV at low irradiances. At $\chi = 10^{-8}$, surface charge persists and requires considerably higher irradiances in order to bring about saturation through screening. Values of χ were selected such that the SPV model approximates our experimental observations for both the GaAs reference surface ($\chi = 3 \times 10^{-2}$) and the surface prepared with n_{15}-SAM ($\chi = 1 \times 10^{-4}$).

In calculating the SPV representing n_{15}-SAM prepared surfaces, the limiting value of δ_n was assumed and reflects the maximum effect (curve shifting left) a reduction of the SRV can induce following passivation, i.e., $S_{\text{eff}} \ll D_p/L_p$ as defined in section 3.4. However, the sensitivity of δ_n to reductions of S_{eff} is small for SI-GaAs, since $S_{\text{eff}}^{\text{SI}} \approx D_p/L_p$ in (8), so the shifting effect is negligible in this case. This low sensitivity highlights the independence of χ in determining the SPV for this material and relaxes the requirement for accurate knowledge of the SRV.

The curves in figure 5 follow in the same manner as figure 4 for n^{+}-GaAs. A value of $\chi \sim 1$ is assigned to the GaAs reference surface and a value of $\chi = 1 \times 10^{-4}$ is assigned to the surface prepared with n_{15}-SAM, assuming again the SRV limited value of δ_n applies in the latter case. The resulting curve shift left is more significant for passivated n^{+}-GaAs, relative to SI-GaAs, as indicated in figure 5 by the opposed arrows, since $S_{\text{eff}}^{\text{n+}} > D_p/L_p$ for the reference surface conditions. Despite these specific differences, the data and model results for n^{+}-GaAs reflect the same general characteristics evident in the case of SI-GaAs, namely, a small to negligible change in the equilibrium surface barrier, yet a significant (100–165 mV) reduction of SPV following thiol treatment at low-level photo-injection.

A similar reduction of the SPV (∼200 mV) has been observed following S_2Cl_2 sulfide passivation of n-doped GaAs(001) by Tomkiewicz *et al* [37]. The equilibrium surface barrier height was not reported in this study, somewhat limiting their conclusions in that a reduction in equilibrium band-bending was assumed. However, their results do provide a reasonable basis of comparison against the n^{+}-GaAs data in figure 5. In addition to the decrease in SPV, the absolute values appear to be accurately reproduced. Their data also show a logarithmic dependence on irradiance, in agreement with the modeling presented here. Given that pinning of the surface FL was not ruled out, we suggest that the Tomkiewicz results may also be interpreted in terms of a reduction in the χ factor.

3.6. Interface dipole effect

In the foregoing analysis, the change in SPV was attributed to a relative increase in the non-equilibrium band-bending following passivation with *n*-alkanethiol SAMs. This was accounted for in the SPV model by a decrease in the hole/electron ratio of carrier capture coefficients when compared to the untreated surface. Consider a reduction of the minority carrier capture cross-section (σ_p), which is consistent with the fitting of χ to the SPV data for both material types, recalling that $\chi \propto \sqrt{\sigma_p/\sigma_n}$, and that is effected by S–GaAs coupling. A large scale reduction of σ_p is implied in the limit

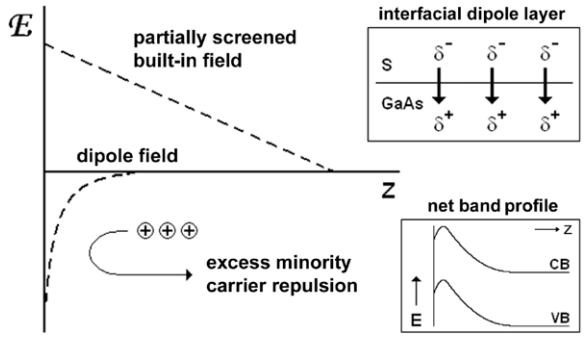

Figure 6. Representation of the electric field profiles associated with: (i) the built-in field of the SCR, partially screened under illumination, and (ii) the penetrating interfacial dipole layer. Insets: interfacial dipole layer formed by S–GaAs covalent bonding (top). Net band profile of the thiol–GaAs interface (bottom). Schematic only, not to scale.

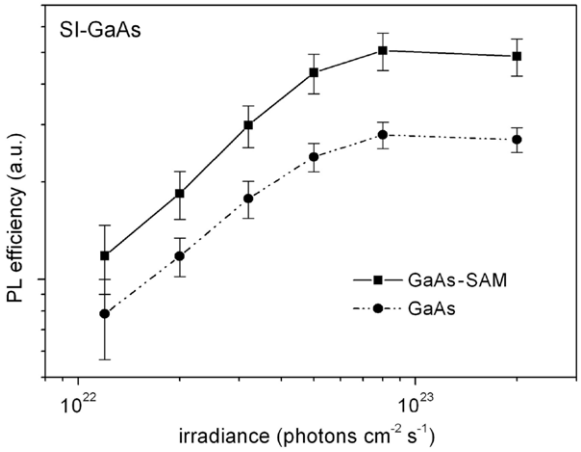

Figure 7. Relative PL efficiency as a function of the excitation power for SI-GaAs before (circles) and after (squares) preparation with n_{15}-SAM. Yield saturation is evident at irradiances above 10^{23} photons cm^{-2} s^{-1}, corresponding to the flat-band condition.

$S_{\text{eff}} \ll D_p/L_p$ used to scale the irradiance for the passivated surfaces, and is consistent with a reduction of SRV that derives from $S_{\text{L}} = \sigma_p \nu_{\text{th},p} N_{\text{t}}$, the well-known expression for Shockley–Read–Hall surface recombination under low level photo-injection as specified for n-type GaAs. Note that a significant reduction of N_{t} is rejected on the basis of strong FL pinning [23]. Regarding a mechanism for the reduction of χ, we propose that a significant factor is electrostatic in nature and results from the interfacial dipole layer formed upon thiol chemisorption, as described in the following.

Thiol may be considered an electron pair donor to a complementary GaAs acceptor state, resulting in a surface complex of bonding molecular orbitals [24]. The S–GaAs adduct thus formed is characterized by a dipole potential with its moment directed into the surface. An interfacial layer of these dipoles will increase the surface work function, as similarly reported by Tomkiewicz *et al* [37], who observed, independently of their SPV data, a work function increase of 0.21 eV after passivation of GaAs(001) with S_2Cl_2. An interfacial dipole layer associated with the SAM will affect the internal potential locally. Specifically, it is proposed that the penetrating field of the S–GaAs dipole layer acts to lower the band levels and invert the band-bending curvature in the near-surface region. The manifestation of such an effect would be determined by: (1) the penetrating field strength relative to the partially screened field of the SCR under photo-injection, and (2) the penetrating field profile, which, as a sum of dipole fields, is dependent on the dipole moment, the inter-dipole distance, and on local domain patterns and disordering defects. As calculated in Natan *et al* [38], the net result of these effects, for bond polarizations on the order of 1 debye and two-dimensional packing densities typical of adsorbed monolayers, is an exponentially decreasing field strength exceeding 10^4 V cm^{-1} at distances up to about 10 nm below the surface. The field strengths associated with the equilibrium surface potentials are also of this magnitude, or greater, in this region and decrease proportionately with SPV in the low-injection regime. This suggests that addition of the interfacial dipole and built-in fields will create a local inversion barrier that retards surface trapping of excess minority carriers. This dipole barrier effectively reduces the surface capture cross-section σ_p of the relevant surface states, and will increase it for σ_n, which is reflected in the model fitting of $\chi \ll 1$ to the SPV data. A schematic of the respective fields, near-surface band structure and the proposed effect on minority carrier capture is provided in figure 6.

An interesting parallel to the concept of field-dependent cross-sections relates to the findings of Prinz and Rechkunov [39], who demonstrated a field-enhanced cross-section effect in the depletion region of semi-insulating GaAs Schottky barriers, specific to the EL2 and other bulk defect centers. For applied field strengths exceeding 10^4 V cm^{-1}, σ_p and σ_n were observed to increase asymmetrically, by up to six orders, with a trend toward $\chi = 1$. Under zero field, χ was reduced by an order of 10^{-2}. Although the details of the Prinz and Rechkunov result do not fit into the framework of the present work directly, at a minimum, they do argue for the field-dependent sensitivity of σ_p and σ_n on the scales discussed and in relation to field strengths of similar magnitude.

4. PL observations and analysis

4.1. PL enhancement in the flat-band regime

The relative PL efficiency versus photon irradiance is plotted in figure 7 for SI-GaAs before and after preparation with n_{15}-SAM. To obtain the PL efficiencies, the measured PL intensities were divided by the transmittances of the neutral density filters used to attenuate the irradiance. A PL enhancement factor of about 1.8× is evident for the thiol-treated surface, relative to the reference surface after etching. Data recorded within a few hours after sample preparation typically yield enhancement factors averaging 1.6(±0.2). An important feature is the saturation of PL yield observed at irradiances above 10^{23} photons cm^{-2} s^{-1}. Considering the magnitude of scale, the PL saturation point agrees well with the saturation point predicted by SPV modeling in figure 4. The two points are expected to coincide; specifically, the PL yield

will saturate when the effective SRV becomes minimized, i.e., when the drift current in the SCR is minimized due to band-flattening. On careful inspection of figure 7, some indication of decreased PL efficiency is evident, as the irradiance increases in the flat-band regime, which may be attributed to Auger recombination processes initiated by the onset of degenerate occupation.

Recall that a discrete distribution of surface state energies was assumed in the context of the AUDM for SPV modeling. In contrast, the disorder-induced gap state (DIGS) model proposes a U-shaped distribution of surface state energies within the band-gap [40]. When reduced to the limit of a discrete level defect, the DIGS model predicts a unitary rate increase of the PL efficiency with excitation power [41]. Inspection of figure 7 below yield saturation indicates that the efficiency rate of increase is 90% for the thiol-treated surface, suggesting that a discrete level defect is playing a significant role.

We now examine the implications of the SPV findings in the context of the PL enhancement using a near-surface model of the excess carrier transport. In n-type material under low-injection conditions, the minority carrier transport equation is [42]

$$\frac{\partial}{\partial t}\Delta p(z,t) = D_p\frac{\partial^2}{\partial z^2}\Delta p - \mu_p\frac{\partial}{\partial z}[\Delta p\mathcal{E}(z)] + I_{\text{rad}}(1-R)\alpha_{\text{ex}}\mathrm{e}^{-\alpha_{\text{ex}}z} - \frac{\Delta p}{\tau_p} \tag{9}$$

where Δp is the excess carrier density, D_p is the diffusion coefficient, μ_p is the carrier mobility, $\mathcal{E}(z)$ is the built-in electric field in the SCR, I_{rad} is the irradiance of the excitation source, R is the surface reflectance, α_{ex} is the absorption coefficient at the excitation wavelength, z is the spatial coordinate normal to the surface, and τ_p is the carrier lifetime. Under steady-state conditions, the time-derivative is zero; consequently, the spatial distribution of excess holes can be found by solution of (9) subject to the following boundary conditions [36],

$$D_p\frac{\partial}{\partial z}\Delta p(z)\bigg|_{z=z_{\text{d}}} = S_{\text{eff}}\Delta p(z_{\text{d}}) \tag{10}$$

$$\Delta p(\infty) = 0. \tag{11}$$

A solution to (9), subject to (10) and (11), can be obtained numerically as a boundary-value problem [42], or can be solved analytically in terms of the dimensionless variable $S_{\text{rv}} = S_{\text{eff}}\tau_p/L_p$ [36]. Note that $\mathcal{E}(z \geqslant z_{\text{d}}) = 0$ in the depletion approximation. Also, generation and transport within the SCR can be ignored if $z_{\text{d}} \ll \alpha_{\text{ex}}$ and $z_{\text{d}} \ll L_p$, where L_p is the diffusion length for holes ($L_p = \sqrt{D_p\tau_p}$) [33], and radiative recombination may ignored in the SCR, which accords with the principle of a dead layer. Once $\Delta p(z)$ is determined, the PL can be obtained by integration of the radiative recombination rate [43],

$$PL \propto \int_{z_{\text{d}}}^{\infty}\frac{\Delta p(z)}{\tau_{\text{r}}}\,\mathrm{d}z \tag{12}$$

where τ_{r} is the radiative lifetime.

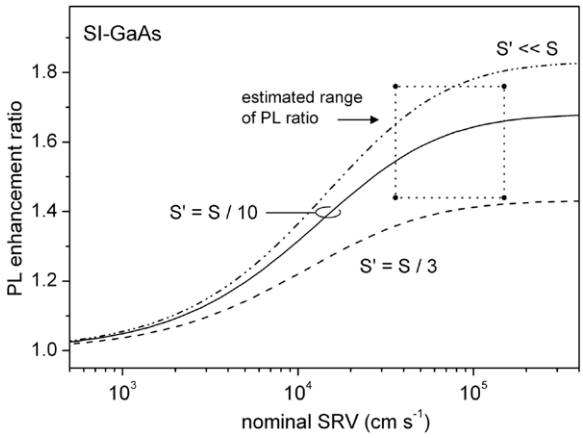

Figure 8. Calculated PL enhancement ratio for SI-GaAs following passivation with n_{15}-SAMs as a function of the nominal SRV (S) before passivation. Curves are computed for values of $S' < S$, indicating the reduced surface value after passivation. The boxed area demarks the parameter space within which the PL ratio may be found.

In the transport model, simulation of the high-injection regime can be approximated by allowing the excess carrier density to exceed the donor concentration and forcing the dead layer to zero. First, the excess carrier density ($\Delta n = n - n_{\text{o}}$) is estimated from (8) and is used to obtain the carrier lifetime,

$$\tau_p = (\beta n + S_{\text{eff}}/L_p)^{-1} \tag{13}$$

where β is the radiative rate constant for GaAs, which is applicable under non-degenerate injection [44]. Since $\beta n \approx S_{\text{eff}}/L_p$ under steady-state high-injection, reduction of S_{eff}/L_p following passivation justifies the simplification that τ_p is approximately constant. The dimensionless value S_{rv} is subsequently determined as a function of S_{eff}, and is substituted in the solution to (9) [36], following which the PL is found by integration of (12). By forming the appropriate PL intensity ratio, the PL enhancement factor (R_{PL}) can be calculated for a specified reduction of S_{eff} following passivation and compared to the experimental data.

Results from the prescribed analysis are plotted in figure 8 as a function of the nominal SRV ($S = S_{\text{eff}}$) corresponding to the etched and untreated surface. Each curve is calculated assuming a specific reduction factor of S following passivation. The solid curve represents a 10× reduction ($S' = S/10$). The dashed curve represents a 3× reduction of S and approximates the lower boundary of R_{PL} subject to the range within which it was observed, which is defined by the boxed area height. The dash-dotted curve was determined using the limiting value $S' \ll S$ and illustrates the upper boundary of R_{PL}. The width of the box in figure 8 spans the uncertainty in the nominal value of S_{eff}. The right boundary is defined by the value of $S_{\text{eff}}^{\text{SI}}$ chosen for SI-GaAs, i.e., the effective value of SRV under low-injection. The left boundary represents the limit under high-injection conditions, using $S_{\text{H}} \approx S_{\text{L}} = C_p N_{\text{t}}$, which is valid for $\chi \ll 1$ since $S_{\text{H}} = C_p N_{\text{t}}/(\chi^2 + 1)$, and is approximated using the following values: $N_{\text{t}} = 2.1 \times 10^{12}$ cm^{-2} as determined in section 3.3, $\nu_{\text{th},p} = 1.8 \times 10^7$ cm s^{-1} for GaAs, and $\sigma_p = 1.0 \times 10^{-15}$ cm^2, which is an approximate value

based on atomic dimensions [33, 45]. The nominal value of S_{eff} will trend left within this space as the drift current in the SCR is minimized under band-flat conditions, but its actual value remains unknown. Consequently, we may only bracket the values of R_{PL} according to an estimated variation of the governing parameters in the model.

4.2. Discussion of PL results

Based on the SPV results, a large scale reduction of χ consistent with a significant reduction of the effective SRV was proposed. A significant reduction of the SRV is evident in the PL enhancement modeling above, namely, the $S' \ll S$ result in figure 8. The conclusions of Lunt *et al* [18], which were based on time-resolved PL measurements observed under photo-saturation conditions following a high-injection pulse, reported an SRV reduction measuring just $3\times$ ($S' = S/3$). Their lower value may have resulted from the transient nature of the time-resolved experiment, or may have been due to a less effective passivation realized with the short-chain thiols that were used. More importantly, their technique did not allow for a distinction to be made between a reduction of $\sigma_{n,p}$ or N_{t}, nor did it exclude the possibility of contraction of the dead layer. Given that the effect of a large scale decrease of σ_p is supported by both the SPV and PL analysis, and that Fermi level pinning has ruled out a significant change in N_{t} [23], the following conclusion is drawn, i.e., it is a thiol-induced reduction of σ_p that is most significant to the PL increase following passivation with alkanethiol SAMs. Note that in order to account for the PL enhancement observed, a dead-layer model explanation would specify a reduction of the equilibrium surface barrier height in excess of 250 meV. This is a substantial degree of electronic passivation that is clearly not supported by our previously reported XPS results.

As a final point consider that, in the above section, we reviewed our results on SI-GaAs only, since measurements of the heavily doped n^+-type material yielded null PL enhancements following thiol treatment. Increases in doping concentration lead to proportionally greater radiative recombination rates. Similarly, there is a proportional increase in the SRV, as the results compiled in Aspnes suggest [35]. However, there is a marked flattening of the SRV increase when the doping concentration becomes degenerate. Evidently, under sufficiently heavy doping, the radiative rate continues to grow but the SRV does not. Since the SRV becomes proportionately smaller, surface related effects become less significant. This can be simulated in the present model by artificially increasing the excess carrier density, though a more accurate result is beyond the reach of the non-degenerate approximation methods used.

5. Conclusions

The electro-optic effects of *n*-alkanethiol SAM formation on GaAs(001) were investigated using SPV, PL and numerical methods. SPV measurements indicated that the residual non-equilibrium surface potentials of samples prepared with n_{15}-SAMs were significantly greater than that of etched GaAs reference surfaces under low-injection conditions. SPV modeling accounted for this in terms of a substantial ($>10^4$) reduction of the hole/electron ratio of carrier capture cross-sections. It was proposed that the formation of an interfacial dipole layer associated with thiol chemisorption retards the hole capture efficiency through near-surface band modifications imparted by penetrating dipole fields.

The PL efficiency following passivation with n_{15}-SAMs was observed to increase about $1.6\times$ for SI-GaAs saturating above irradiances in agreement with SPV modeling. Carrier transport representation of the PL enhancement supported the SPV data within the uncertainty of the governing surface parameters. It was concluded that, under Fermi level pinning conditions, a thiol-induced reduction of the minority carrier surface capture cross-section is the significant factor affecting PL increases following passivation with alkanethiol SAMs.

Acknowledgments

Funding for this research was provided by the Natural Sciences and Engineering Research Council of Canada, the Canada Research Chair in Quantum Semiconductors Program and the National Research Council of Canada Graduate Student Scholarship Supplement Program.

References

[1] Ahktari-Zavareh A, Li W, Kavanagh K L, Trionfi A J, Jones J C, Reno J L, Hsu J W P and Talin A A 2008 *J. Vac. Sci. Technol.* B **26** 1597–601
[2] Lee K, Lu G, Facchetti A, Janes D B and Marks T J 2008 *Appl. Phys. Lett.* **92** 123509
[3] Nesher G, Shpaisman H and Cahen D 2007 *J. Am. Chem. Soc.* **129** 734–5
[4] Loo Y, Lang D V, Rogers J A and Hsu J W P 2003 *Nano Lett.* **3** 913–7
[5] Wu D G, Ashkenasy G, Shvarts D, Ussyshkin R V, Naaman R, Shanzer A and Cahen D 2000 *Angew. Chem. Int. Ed.* **39** 4496–500
[6] Cahen D, Naaman R and Vager Z 2005 *Adv. Funct. Mater.* **15** 1571–8
[7] Francia G D, Ferrara V L, Manzo S and Chiavarini S 2005 *Biosens. Bioelectron.* **21** 661–5
[8] Duplan V, Miron Y, Frost E, Grandbois M and Dubowski J J 2009 *J. Biomed. Opt.* **14** 054042
[9] Nakagawa O S, Ashok S, Sheen C W, Märtensson J and Allara D L 1991 *Japan. J. Appl. Phys.* **30** 3759–62
[10] Aqua T, Cohen H, Vilan A and Naaman R 2007 *J. Phys. Chem.* C **111** 16313–8
[11] Jun Y, Zhu X and Hsu J W P 2006 *Langmuir* **22** 3627–32
[12] McGuiness C L, Blasini D, Masejewski J P, Uppili S, Cabarcos O M, Smilgies D and Allara D L 2007 *ACS Nano* **1** 30–49
[13] Voznyy O and Dubowski J J 2008 *Langmuir* **24** 13299–305
[14] Shaporenko A, Adlkofer K, Johansson L S O, Tanaka M and Zharnikov M 2003 *Langmuir* **19** 4992–8
[15] Kim C, Marshall G M, Martin M, Bisson-Viens M, Wasilewski Z and Dubowski J J 2009 *J. Appl. Phys.* **106** 083518
[16] Adlkofer K, Duijs E F, Findeis F, Bichler M, Zrenner A, Sackmann E, Abstreiter G and Tanaka M 2002 *Phys. Chem. Chem. Phys.* **4** 785–90
[17] Ding X, Moumanis K, Dubowski J J, Tay L and Rowell N L 2006 *J. Appl. Phys.* **99** 054701

[18] Lunt S R, Ryba G N, Santangelo P G and Lewis N S 1991 *J. Appl. Phys.* **70** 7449–67
[19] Dorsten J F, Maslar J E and Bohn P W 1995 *Appl. Phys. Lett.* **66** 1755–7
[20] McGuiness C L, Shaporenko A, Zharnikov M, Walker A V and Allara D L 2007 *J. Phys. Chem.* C **111** 4226–34
[21] Budz H A, Biesinger M C and LaPierre R R 2009 *J. Vac. Sci. Technol.* B **27** 637–48
[22] Wieliczka D M, Ding X and Dubowski J J 2006 *J. Vac. Sci. Technol.* A **24** 1756–9
[23] Marshall G M, Bensebaa F and Dubowski J J 2011 *Appl. Surf. Sci.* **257** 4543–6
[24] Seker F, Meeker K, Kuech T F and Ellis A B 2000 *Chem. Rev.* **100** 2505–36
[25] Darling R B 1993 *J. Appl. Phys.* **74** 4571–89
[26] Martin G M, Farges J P, Jacob G, Hallais J P and Poiblaud G 1980 *J. Appl. Phys.* **51** 2840–52
[27] Spicer W E *et al* 1988 *J. Vac. Sci. Technol.* B **6** 1245–51
[28] McGuiness C L, Shaporenko A, Mars C K, Uppili S, Zharnikov M and Allara D L 2006 *J. Am. Chem. Soc.* **128** 5231–43
[29] Marshall G M, Lopinski G P, Bensebaa F and Dubowski J J 2009 *Langmuir* **25** 13561–8
[30] Aphek O B, Kronik L, Leibovitch M and Shapira Y 1998 *Surf. Sci.* **409** 485–500
[31] Garrett C G B and Brattain W H 1955 *Phys. Rev.* **99** 376–87
[32] Johnson E O 1958 *Phys. Rev.* **111** 153–66
[33] Kronik L and Shapira Y 1999 *Surf. Sci. Rep.* **37** 1–206
[34] Schroder D K 2001 *Meas. Sci. Technol.* **12** R16–31
[35] Aspnes D 1983 *Surf. Sci.* **132** 406–21
[36] Mettler K 1977 *Appl. Phys.* **12** 75–82
[37] Tomkiewicz P, Arabasz S, Adamowicz B, Miczek M, Mizsei J, Zahn D, Hasegawa H and Szuber J 2009 *Surf. Sci.* **603** 498–502
[38] Natan A, Kronik L, Haick H and Tung R 2007 *Adv. Mater.* **19** 4103–17
[39] Prinz V Y and Rechkunov S N 1983 *Phys. Status Solidi* b **118** 159–66
[40] Hasegawa H and Ohno H 1986 *J. Vac. Sci. Technol.* B **4** 1130–8
[41] Gfroerer T H 2000 Photoluminescence in analysis of surfaces and interfaces *Encyclopedia of Analytical Chemistry: Applications, Theory, and Instrumentation* ed R A Meyers (New York: Wiley) pp 9209–31
[42] Geisz J F, Kuech T F and Ellis A B 1995 *J. Appl. Phys.* **77** 1233–40
[43] Vilms J and Spicer W E 1965 *J. Appl. Phys.* **36** 2815–21
[44] Lambert B, Sermage B, Deveaud B, Clerot F, Chomette A and Regreny A 1990 *Surf. Sci.* **228** 210–2
[45] Baca A G and Ashby C I H 2005 *Fabrication of GaAs Devices* (London: Institution of Electrical Engineers) p 84